New Methods to Infer Snow Albedo From the MISR Instrument With Applications to the Greenland Ice Sheet

Julienne C. Stroeve and Anne W. Nolin

***Abstract*—Snow-covered surfaces have a very high surface albedo, thereby allowing little energy to be absorbed by the snowpack. As the snowpack ages and/or begins to melt, the snow albedo decreases and more solar energy is absorbed by the snowpack. Therefore, accurate estimation of snow albedo is essential for monitoring the state of the cryosphere. This paper examines the retrieval of snow albedo using data from the Multi-angle Imaging SpectroRadiometer (MISR) instrument over the Greenland ice sheet. Two different methods are developed and examined to derive the snow albedo: one based on the spectral information from MISR and one utilizing the angular information from the MISR instrument. The latter method is based on a statistical relationship between *in situ* albedo measurements and the MISR red channel reflectance at all MISR viewing angles and is found to give good agreement with the ground-based measurements. Good agreement is also found using the spectral information, although the method is more sensitive to instrument calibration, snow bidirectional reflectance distribution function (BRDF) models, and narrowband-to-broadband relationships. In general, using either method retrieves snow surface albedo values that are within about 6% of that measured at the stations in Greenland.**

***Index Terms*—Greenland, Multi-angle Imaging SpectroRadiometer (MISR), snow albedo.**

I. Introduction

SURFACE albedo is an important climate parameter, as it influences the amount of solar radiation absorbed by the surface. For snow-covered surfaces, the albedo may be greater than 0.80, thereby allowing very little solar energy to be absorbed by the snowpack. As the snow ages and/or begins to melt, the albedo is reduced considerably, leading to enhanced absorption of solar radiation which further reduces the surface albedo. Consequently, snow melt comprises an unstable, positive feedback component of the earth's climate system, which amplifies small perturbations to that system.

Vast expanses of the earth's surface are covered by snow, such as the Greenland and Antarctic ice sheets. These ice sheets cool the climate by affecting the local energy balance through reduced absorption of solar radiation. Since most energy for melting is supplied by solar radiation in these regions, knowledge of the surface albedo is essential for energy and mass balance studies. The surface albedo is not only needed to derive the energy balance, it is also an indicator of many physical aspects of the snow surface, such as snow thickness, grain size, and water content.

Satellite remote sensing offers a means for measuring and monitoring the surface albedo of snow-covered surfaces in remote places such as the polar regions. Several studies have attempted to estimate the albedo in the Arctic using data from the National Oceanic and Atmospheric Administration (NOAA) Advanced Very High Resolution Radiometer (AVHRR) (e.g., [1]–[3]). Snow albedo is also one of the standard products to be generated in the near future from data acquired by the Moderate Resolution Imaging Spectroradiometer (MODIS) instrument flown on the Terra and Aqua satellites [4]. Snow albedo from instruments such as AVHRR and MODIS rely on using variations in spectral reflectance to derive the albedo. With the Multi-angle Imaging SpectroRadiometer (MISR), also flown on Terra, the possibility exists to use the angular signatures in addition to spectral signatures for high-resolution snow albedo retrievals, as well as many other potential applications for cryospheric research [5].

This study evaluates clear-sky snow surface albedo retrievals from the MISR instrument through comparisons with ground-based albedo measurements obtained in Greenland. Although surface albedo is routinely retrieved as part of the MISR operational processing system, the quality of the albedo is dependent on the accuracy of the aerosol retrievals (e.g., [1]) which are used as input to the atmospheric correction. Over bright, homogeneous targets such as the Greenland ice sheet, the MISR aerosol retrievals are currently in very early states of checkout and validation. Therefore, in order to investigate the information content of MISR data with respect to snow albedo, we developed and examined two different techniques for retrieving the surface albedo: one using the angular information provided by the MISR data and the other based on the spectral information from MISR. Data from automatic weather stations in calendar years 2000 and 2001 provide measurements of atmospheric variables needed for the atmospheric correction, and they provide the ground-based measurements with which to compare coincident clear-sky satellite albedo retrievals.

In discussing the albedo retrieval methodology from satellite, it is helpful to define the different reflectance/albedo terms that

Manuscript received October 16, 2001; revised May 2, 2002. This work was supported by NASA Grant NAG5-6462.

The authors are with The National Snow and Ice Data Center (NSIDC), Cooperative Institute for Research in Environmental Sciences (CIRES), University of Colorado, Boulder, CO 80309-0449 USA (e-mail: stroeve@kodiak.colorado.edu).

Publisher Item Identifier 10.1109/TGRS.2002.801144.

will be used throughout the paper. These are defined according to [6].

1) *Bidirectional Reflectance Distribution Function (BRDF):* Surface-leaving radiance divided by incident irradiance from a single direction.
2) *Bidirectional Reflectance Factor (BRF):* Observed radiance divided by the radiance from a perfect Lambertian reflector, under conditions in which the illumination is from a single direction. This term is used in this paper to refer to both the top-of-the-atmosphere (TOA) and at the surface.
3) *Hemispherical-Directional Reflectance Factor (HDRF):* Surface-leaving radiance divided by radiance from a perfect Lambertian reflector, under conditions of ambient (direct and diffuse) illumination. Atmospheric correction of satellite measurements for direct and diffuse transmission, but not for diffuse irradiance at the surface, yields the HDRF.
4) *Bihemispherical Reflectance (BHR):* The surface albedo, as measured by an albedometer at the surface, where the incident illumination is both direct and diffuse.

II. Study Site

The surface albedo is derived from the MISR data at five different study sites in Greenland. These sites are part of a network of automatic weather stations (AWS) that compose the Greenland Climate Network (GC-Net) [7]. Presently, 21 AWS are operational, providing measurements of the surface radiation balance, turbulent fluxes, conductive heat flux in the snow pack, as well as profiles of temperature, humidity, wind speed and direction, snow height, and pressure. The sites used for the intercomparison are shown in Fig. 1 and are as follows.

1) *ETH/CU:* This station, also known as the Swiss Camp, is located at the equilibrium line altitude on the western side of the ice sheet [69.59°N, 49.27°W; 1150 m above sea level (a.s.l.)].
2) *JAR:* This station is situated in the ablation region downstream from the ETH/CU camp (69.50°N, 49.69°W; 962 m a.s.l.).
3) *Summit:* This station is located at the highest point of the ice sheet (72.58°N, 38.50°W; 3150 m a.s.l.).
4) *Humboldt:* This is situated in the northwestern part of the ice sheet in a region of high annual accumulation (78.53°N/56.83°W; 1995 m a.s.l.).
5) *TUNU-N:* This is located in a relatively low accumulation region of the ice sheet in the northeast (78.02°N, 33.99°W; 2113 m a.s.l.).

All the AWS employ LI–COR 200SZ photoelectric diodes to measure incoming and reflected solar radiation in the 0.4–1.1-μm wavelength range. This spectral range does not cover the entire solar spectrum, such as what is typically measured by an albedometer or a set of pyranometers (e.g., 0.3–3.5 μm). Relative calibration of the LI–COR-measured surface albedo with those measured from Eppley precision spectral pyranometers (PSP) at the ETH/CU camp show a positive bias of around 4% [8]. However, this bias may not be applicable to other stations, since different atmospheric and surface conditions will affect the relationship. For example,

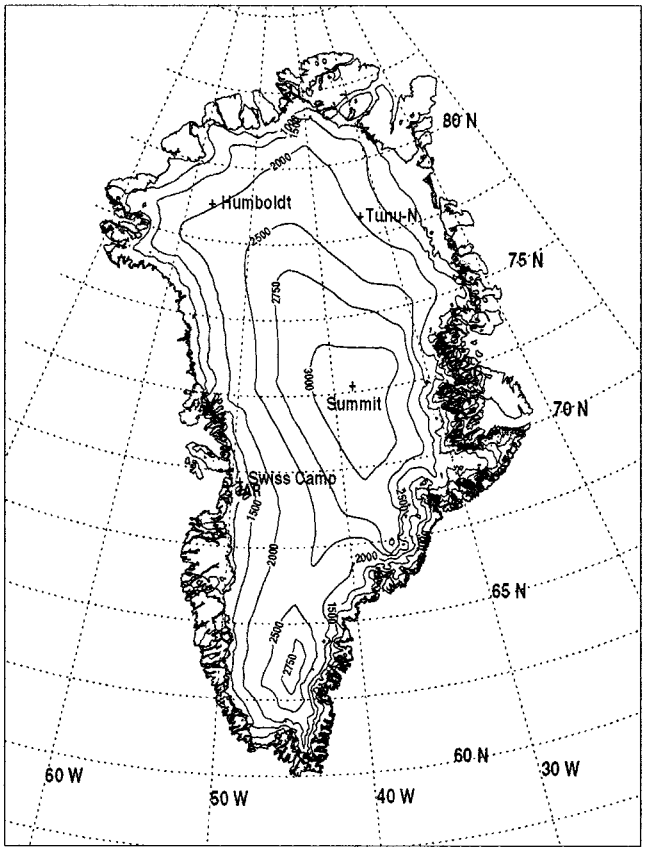

Fig. 1. Map of the Greenland ice sheet showing the AWS locations used for the albedo comparisons.

based on model simulations of snow albedo using a standard arctic summer atmospheric model, the difference between LI–COR and PSP albedo for snow grain sizes of 100, 500, and 1000 μm is 6.9, 8.9, and 10.8%, respectively, at a solar zenith angle of 65°. Thus, we stress here that caution is needed when making comparisons between the LI–COR albedo and the broadband albedo being derived from the MISR spectral data. In this study, we will be using the narrowband-to-broadband conversion coefficients from [9], and, therefore, the resulting surface albedo will correspond to slightly different spectral ranges than the LI–COR measurements. Finally, clear skies are estimated from visual inspection of the satellite data and from the AWS data by comparing measured and modeled (clear-sky) incoming solar radiation at the station (see [8] for more detailed information on this procedure).

III. MISR Satellite Data

The MISR instrument is on board the NASA Earth Observing System (EOS) Terra satellite which was launched December 18, 1999. MISR uses nine discrete cameras pointed at fixed angles, one looking straight down (nadir), as well as well as four viewing angles in both the forward (f) and aftward (a) directions along the spacecraft ground track. The four angles on either side of nadir are 26.1°, 45.6°, 60.0°, and 70.5°, referred to as the A, B, C, and D cameras, respectively. The nadir camera is called the An camera. For this work, the MISR L1B2T (terrain-registered) TOA-scaled radiance data are used. The L1B2 data are

in the Space Oblique Mercator (SOM) grid, such that each orbital path is gridded into 180 blocks. The red channel data are at 275-m resolution for all cameras, as are the blue, green, red, and near-infrared channels of the nadir camera. All other channels (in the instrument's Global Mode) are at 1.1-km resolution.

For each region of interest, the following cameras and channels were extracted for a 50-by–50 pixel subregion centered on each station: Df–red, Cf–red, Bf–red, Af–red, An–blue, An–green, An–red, An–nir, Aa–red, Ba–red, Ca–red, and Da–red (see Table I for channel wavelengths). The subset data are converted from TOA-scaled radiances to TOA BRF using TOA solar irradiance and solar zenith angle data supplied with the MISR imagery. Table II summarizes dates of acquisition of MISR data used in this study.

TABLE I
CENTER WAVELENGTH OF SPECTRAL CHANNELS FOR MISR DATA USED IN THIS STUDY

Sensor	Channel 1 (μm)	Channel 2 (μm)	Channel 3 (μm)	Channel 4 (μm)
MISR	0.446	0.558	0.672	0.867

TABLE II
DATES OF ACQUISITION OF MISR DATA USED IN THIS STUDY

Sensor	JAR and ETH/CU	Summit	Humboldt	TUNU-N
MISR	07/20/00	08/25/00	08/06/01	05/16/01
	08/12/00	05/31/01	08/22/01	07/19/01
	06/28/01	06/09/01	08/27/01	07/30/01
	07/07/01	06/11/01		08/20/01
	07/25/01	07/02/01		08/31/01
	07/30/01	07/09/01		
	08/08/01	07/27/01		
		08/19/01		

IV. CLEAR-SKY ALBEDO METHODOLOGY

Albedo, as defined here, is a physical property of the coupled surface–atmosphere system. The broadband surface albedo at a specific solar zenith angle θ_o is defined as the fraction of the incoming solar irradiance reflected back to the sky from the earth's surface. It can be expressed as

$$\alpha(\mu_o) = \frac{\int_{\lambda_1}^{\lambda_2} \rho(\mu_o, \lambda) S(\mu_o, \lambda) d\lambda}{\int_{\lambda_1}^{\lambda_2} S(\mu_o, \lambda) d\lambda} \tag{1}$$

where $\rho(\mu_o, \lambda)$ and $S(\mu_o, \lambda)$ represent the spectral albedo and the downwelling solar irradiance at the surface at $\mu_o = \cos(\theta_o)$ and wavelength λ, respectively.[1] Integrated over the solar spectrum (0.30–3.5 μm), it gives the broadband surface albedo. This is what is typically measured using an albedometer.

What the MISR measurement provides is the TOA BRF, which is dependent upon the viewing geometry of the satellite. The surface albedo under "clear skies" can be derived from reflectance measurements made by satellite, providing a correction for the intervening atmosphere is made. Typically, other steps are needed, since the narrowband channels of satellite instruments generally only represent a fraction of the solar spectrum and are dependent upon the specific viewing geometry of the sun-sensor. The methodology used to derive the broadband albedo from the MISR spectral information is the same as described in [1] and is summarized in Section IV-A. Section IV-B discusses the methodology used to derive the surface albedo from the MISR angular information.

A. Broadband Albedo From Spectral Information

The following discusses the methodology used in deriving the surface albedo using the MISR spectral information for the nadir camera. The methodology can also be applied to off-nadir views. The following steps are discussed in more detail:

1) correction for atmospheric effects;
2) correction for anisotropic reflection at the surface;
3) calculation of the spectrally integrated albedo.

[1] $\rho(\mu_o, \lambda) = (1/\pi \int_0^1 \int_0^{2\pi} \int_0^1 \int_0^{2\pi} R(-\mu, \mu', \phi, \phi', \lambda) I(\mu', \mu_o, \phi', \phi_o, \lambda) \mu\mu' d\mu' d\phi' d\mu d\phi) / (\int_0^1 \int_0^{2\pi} I(\mu', \mu_o, \phi', \phi_o, \lambda) \mu' d\mu' d\phi')$, where $\mu = \cos(\theta)$, ϕ the azimuth angle, $R(-\mu, \mu', \phi, \phi', \lambda)$ the surface spectral bidirectional reflectance factor (BRF), and $I(\mu', \mu_o, \phi', \phi_o, \lambda)$ the total downward radiance (direct + diffuse). Primed quantities refer to reflection angles.

1) Atmospheric Correction: Although the atmosphere is relatively thin over the Greenland ice sheet, atmospheric attenuation of radiation remains significant in the visible and near-infrared wavelengths [1]. Atmospheric correction for MISR is performed using the 6S radiative transfer model [10]. Since the model was not specifically designed with the polar regions in mind, additions were made to the radiative transfer model which included the following:

1) addition of standard Arctic summer and winter atmospheric profiles;
2) spectral albedo of new and old snow;
3) snow BRDF for each of the MISR channels.

For comparisons with station data, the 6S radiative transfer model is run only for the center pixel for each region extracted around the station location. Based on *in situ* optical depth measurements made at the ETH/CU station, an aerosol optical depth of 0.06 is assumed for this station and a value of 0.08 at JAR. At the other stations, aerosol optical depths are scaled according to surface elevation and are 0.01 for Summit and 0.04 for Humboldt and TUNU-N. Ozone and water vapor are taken from a standard arctic summer atmospheric profile assuming surface elevations according to each site.

Using the satellite measurement, an atmospherically corrected reflectance is obtained in 6S using the following equation:

$$r_{\rm ac}(-\mu, \mu_o, \phi, \phi_o) = \frac{a}{1 + Sa} \tag{2}$$

with

$$a = \frac{\frac{R_{\rm sat}(-\mu, \mu_o, \phi, \phi_o)}{T_g} - R_{\rm atm}(-\mu, \mu_o, \phi, \phi_o)}{T(\mu_o) T(-\mu)} \tag{3}$$

where

$r_{\rm ac}$ atmospherically corrected satellite measurement at a specific solar zenith angle $\mu_o = \cos(\theta_o)$, solar azimuth angle ϕ_o, satellite viewing zenith angle $\mu = \cos(\theta)$, and satellite viewing azimuth angle ϕ [the

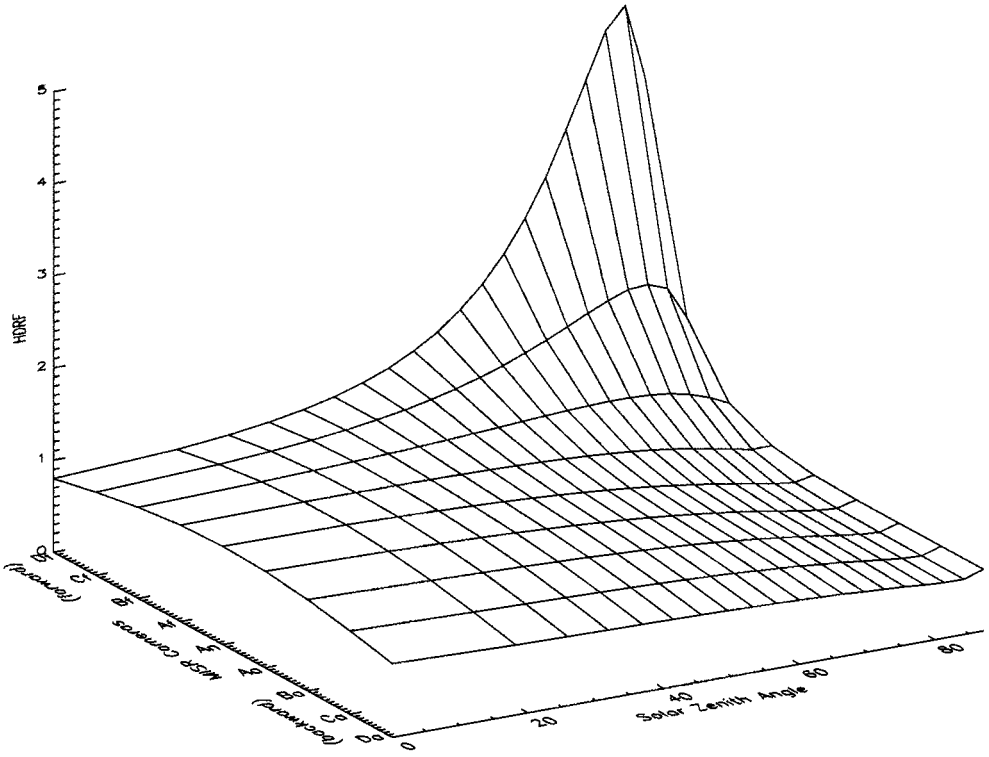

Fig. 2. Modeled surface HDRF for the MISR red channel at the nine MISR discrete viewing angles. Model inputs include snow grain size of 100 μm, arctic summer atmospheric model for water vapor and ozone, and continental aerosol model with aerosol optical depth of 0.01.

latter is also referred to as the surface hemispherical directional reflectance factor (HDRF)];

$R_{\rm sat}$ satellite BRF measurement corresponding to the TOA;

$R_{\rm atm}$ BRF due to atmospheric reflectance only;

T_g dual-path atmospheric transmission due to gaseous absorption only;

$T(-\mu)$ total (direct + diffuse) upwelling transmittance due to scattering only;

$T(\mu_o)$ total (direct + diffuse) downwelling transmittance due to scattering only;

S spherical albedo of the bottom of the atmosphere.

All these parameters are obtained from running the 6S radiative transfer model and are used to derive the surface albedo for each pixel in the subregions using (2) and (3) and assuming that atmospheric conditions and sun-sensor angles remain constant over the subregion.

2) Anisotropic Correction: Field measurements and model simulations show that snow reflects incoming solar radiation anisotropically [11]. Fig. 2 shows modeled snow HRDF assuming a grain size of 100 μm at each of the nine MISR cameras for the red wavelength channel. The strength of anisotropy is more pronounced at higher solar zenith angles, and thus anisotropy becomes significant in the polar regions. Even at nadir viewing angles, the assumption of a Lambertian surface will cause the albedo to be underestimated. For example, at a solar zenith angle of 75°, the albedo calculated using the nadir reflectance is about 0.2 lower than its actual value.

To correct for the angular anisotropy of the snow surface, the HDRF of the snow surface is simulated using a radiative transfer model. The Mie scattering parameters for ice grains of a specified radius are input to the *discrete ordinates radiative transfer* (DISORT) model [12]. DISORT computes the surface HDRF and albedo for specified viewing and solar geometries, as well as the proportions of diffuse and direct illumination. The ratio of the albedo to the HDRF becomes the conversion factor by which the satellite-derived HDRF is then multiplied to obtain the spectral surface albedo for each satellite channel.

For each image to be processed, the direct and diffuse components are obtained using the 6S atmospheric radiative transfer model. The direct and diffuse components for each satellite channel and specific sun-sensor angular geometry are then input into DISORT to derive the conversion factors for each region of interest. In running the DISORT model, a snow grain size of 250 μm was assumed when measurements were otherwise not available. This value is based on the average grain sizes measured at the ETH/CU camp during periods of no melt. For snow conditions in July and August near the ETH/CU and JAR stations, it is likely that much larger grain sizes occur because of aged snow and/or snow melt.

3) Narrowband-to-Broadband Conversion: In general, a linear relationship between the narrowband and the broadband albedo is used (e.g., [1], [9], [13]–[15], and many others) so that the broadband albedo is derived from the following type of equation:

$$\text{broadband} = a_o + b_1 ch_1 + b_2 ch_2 + \cdots + b_n ch_n + \varepsilon \quad (4)$$

where $a_o, b_1, b_2, \ldots, b_n$ are regression coefficients derived from multiple linear regression on the satellite channels ch_i versus the broadband albedo.

The regression coefficients in (4) are not only dependent on surface conditions but are also dependent upon atmospheric conditions [e.g., see (1)]. The downward irradiance distribution at the bottom of the atmosphere is the weighting function for converting the narrowband albedos to broadband albedos. Thus, a relationship developed under a specific surface/atmospheric condition may not be valid under different conditions from which the relationship was developed. This is one reason why published narrowband-to-broadband relationships differ widely.

Another reason why narrowband-to-broadband relationships differ widely is because the independent variables $ch_1 \cdots ch_n$ are highly interdependent. This is referred to as *multicollinearity*. In this situation, the sampling distributions of the estimated regression coefficients can become very broad, with the consequence that a forecasting equation may perform badly when implemented on future data, independent of the training sample. Unfortunately, there is no consensus among statisticians as to what remedies are appropriate when severe multicollinearity is present. For this study, we choose to test the MISR narrowband-to-broadband albedo model of [15]. This model is based on extensive radiative transfer simulations of spectral and broadband albedo for different surface types, including snow.

B. Broadband Albedo From Angular Information

The advantage of the MISR instrument is that the variation of surface reflectance with viewing and illumination angle is another source of information contained within the data besides the spectral content. This information could be used, for example, to invert a snow BRF model so that the snow BRDF and, hence, albedo can be derived from a limited number of observations, such as what is typically done for land surfaces (e.g., [16]–[18], among many others). Under the assumption of an empirical surface BRDF model and retrieved values for aerosol optical properties, it is also possible to use angular information within the MISR data to directly compute the surface albedo. This is the approach taken in the operational MISR land surface products.

We start with the red channel multiangle observations that have been atmospherically corrected (e.g., the HDRF) using the method discussed previously, and we then attempt to derive a statistical model relating the HDRF to the surface albedo. In selecting variables for input into the linear regression model, primary consideration is given to those variables most directly related to the surface albedo. Generally, the relationship between the surface albedo and the shape of the HDRF shown in Fig. 2 depends on both the solar zenith angle and the snow grain size. However, grain size is typically not known and, therefore, cannot be used as a predictor variable.

Here, we use a forward-screening linear regression model to select the predictor variables. The first parameter used is the area under the red spectral channel HDRF curve in the principal plane for each station analyzed. The model then searches through the remaining variables (e.g., solar zenith angle, red channel spectral reflectance at all viewing angles, and nadir spectral reflectance in the blue, green, red, and NIR channels) and selects the ones providing the best improvement in the squared correlation. If the improved explained variance exceeds a threshold of 5%, the variable is included in the multiple linear regression. Using this technique, three predictor variables are used:

1) integral of red HDRF over all viewing angles (both forward and aftward directions);
2) cosine of the solar zenith angle;
3) nadir NIR surface reflectance.

Since we do not have enough clear-sky MISR images to construct a regression model (we currently only have 29 MISR clear-sky images over Greenland) and then use that model on independent MISR data to predict the albedo, a "Bootstrap" approach is used. In this approach, a regression model is derived using all the stations except the one to be predicted. This is done for each station in turn, resulting in 29 different regression models. Next, the surface albedo is predicted at each station location using the regression model based on data from all the other stations. Note, that in deriving the regression models, regression is performed with the LI–COR-measured surface albedo, and, thus, the broadband albedo predicted using this method corresponds to the spectral range of the LI–COR measurement (0.4–1.1 μm).

V. Results

Fig. 3(a)–(e) compares MISR broadband albedo estimates with ground-based measurements at JAR, ETH/CU, Summit, Humboldt, and TUNU-N, respectively. Shown in (3) are the albedo estimates derived using both the multispectral and multiangular approaches determined by averaging ten pixels around the station. At JAR, the surface albedo is seen to decrease dramatically between July and August as a result of surface melting. The *in situ* albedo varies from a dry-snow albedo of around 0.83 to a bare-ice albedo of 0.33. The satellite-derived albedo estimates using either method pick up the decrease in surface albedo observed at the station. The largest differences between the *in situ*- and satellite-derived albedos occur on August 12, 2000. One reason for the discrepancy could be that the surface is quite inhomogeneous around the station during the ablation season. Fig. 4(a) shows an example of the snow conditions found around the JAR and ETH/CU stations on August 12, 2000. Summer melt is active in this region, and several melt ponds are evident near the stations. Because of the inhomogeneity of the surface during the summer melt period, it is difficult to compare the ground-based measurements with the satellite measurements. Even so, the satellite-retrieved albedo values are in overall good agreement with the *in situ* measurements at this site. The multiangular approach results in albedo values that are on average within 3% of the station measurements. The multispectral approach has mean differences on the order of 13%. However, we expect a positive bias of the LI–COR albedo compared to the "broader" albedo being derived with this method. During melting-snow conditions, such as those found at this site, the bias between the LI–COR and broadband albedo could be on the order of nearly 11% (e.g., large grain sizes during melt). Therefore, the differences in albedo with this approach may be more on the order of 2–3%.

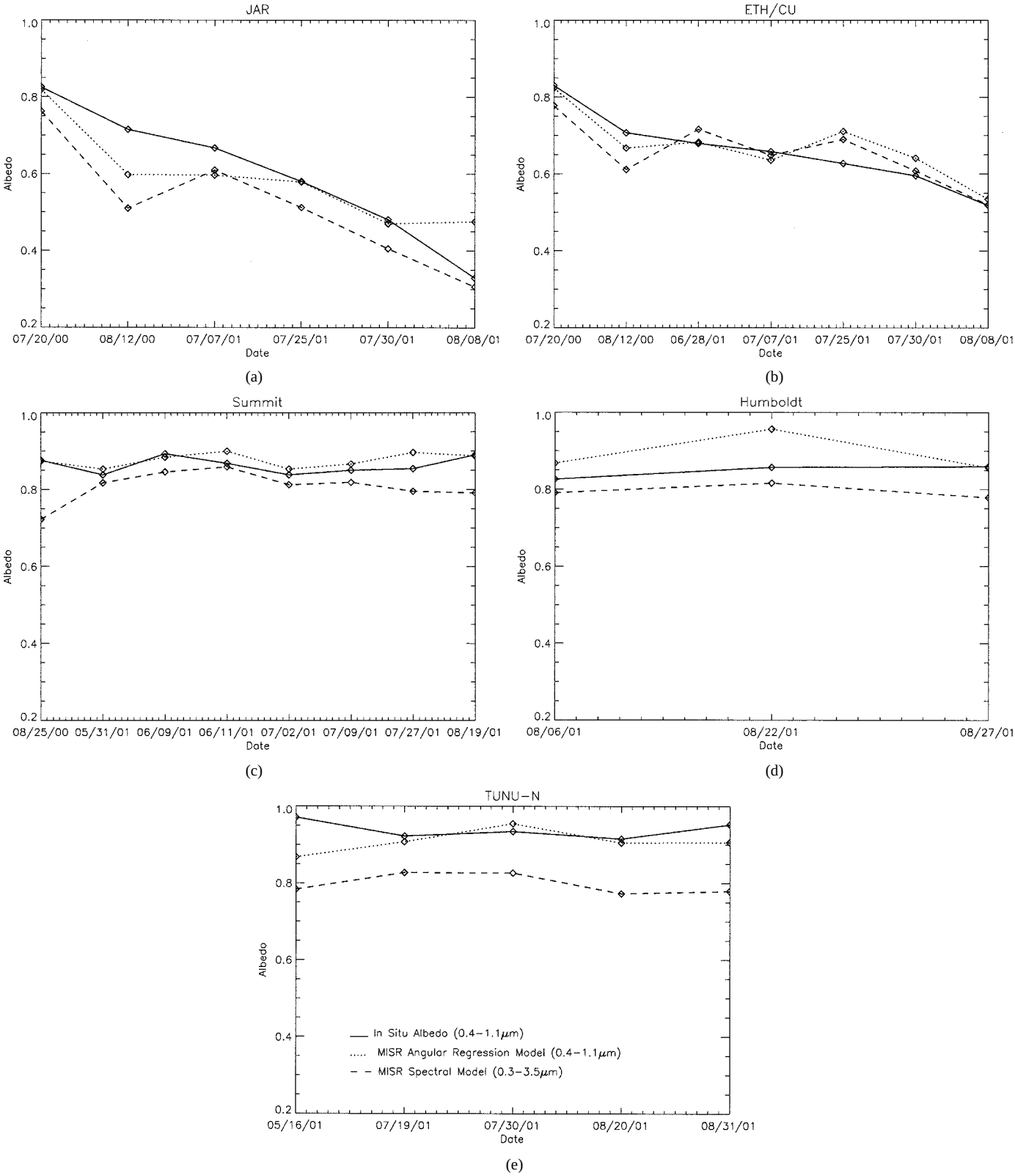

Fig. 3. MISR-derived and LI–COR-measured surface albedo at (a) JAR, (b) ETH/CU, (c) Summit, (d) Humboldt, and (e) TUNU-N. MISR-derived albedos using both the spectral method (dotted line) and the angular method (dashed line) are shown.

At ETH/CU, the albedo is also found to decrease during the summer months as a result of snow melt, although the decrease in albedo is not quite as extreme as at JAR (*in situ* albedo ranges from 0.83–0.52). At this station, the satellite-derived surface albedos are within 2% of the *in situ* measurements using either method. However, we would expect the multispectral method to result in surface albedos that are on the order of 6% less than the *in situ* measurements. It is unclear why at times this method results in surface albedos greater than the station measurements. However, it is entirely possible that there is localized melting at

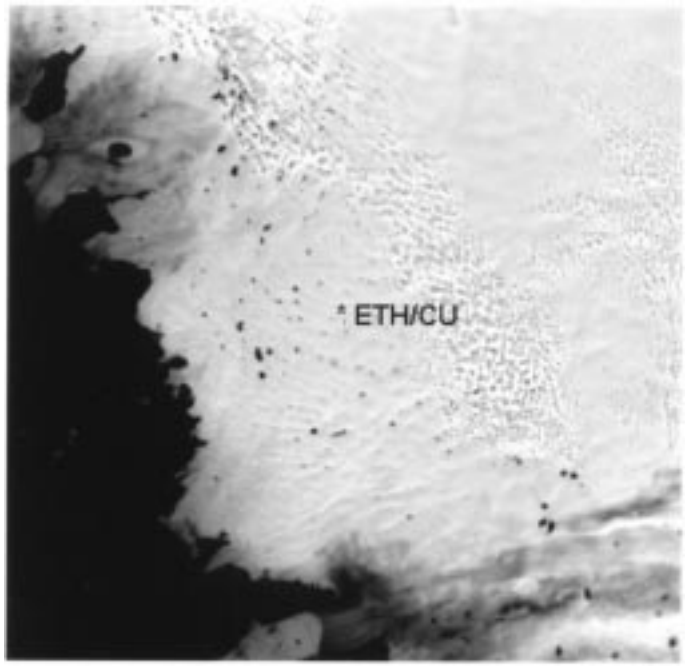

(a)

(b)

Fig. 4. (a) MISR nadir red channel image near the ETH/CU and JAR stations on August 12, 2000. (b) MISR nadir red channel image near the Summit site on August 25, 2000. Clouds are visible in both images. Notice also the many melt ponds near the ETH/CU station.

the station that is not represented in the larger footprint size of the satellite measurement, which could cause the *in situ* measurement to be less than the satellite measurement.

At Summit the surface is fairly homogenous, and the albedo does not vary much: *in situ* albedo ranges from 0.84–0.89 [e.g., see Fig. 4(b)]. Conversely, we expect better agreement between the *in situ*- and satellite-derived surface albedo at Summit than at either JAR or ETH/CU. In general this is indeed the case. The multiangular approach shows very good agreement with the station measurements (less than 2% difference), and the multispectral approach shows differences on the order of 6%. Again, given the positive bias of the LI–COR measurements compared to the broader surface albedo being derived using the multispectral method (bias around 6% for grain size of 250 μm), the agreement is also good using this approach.

At Humboldt, the multispectral method results in surface albedos that are approximately 6% less than the *in situ* measurements. This is similar to the offset observed at Summit. Snow conditions are also similar to Summit, with the *in situ* albedo ranging from 0.83–0.86. The multiangular method shows good agreement with the ground-based measurements except on August 22, 2001. On that date, it appears that the multiangle regression model does not perform well.

TABLE III
MAXIMUM AND MEAN DIFFERENCES BETWEEN THE MISR-DERIVED ALBEDO AND *IN SITU* MEASUREMENTS AT JAR, ETH/CU, SUMMIT, HUMBOLDT, AND TUNU-N. DIFFERENCES ARE OBTAINED BY SUBTRACTING THE SATELLITE ESTIMATE FROM THE *IN SITU* MEASUREMENT. MISR1 REFERS TO THE SURFACE ALBEDO DERIVED USING THE MISR SPECTRAL INFORMATION. MISR2 REFERS TO THE SURFACE ALBEDO DERIVED USING THE MISR ANGULAR INFORMATION

Station	MISR1 Max	MISR1 Mean	MISR1 Std. Dev.	MISR2 Max	MISR2 Mean	MISR2 Std. Dev.
JAR	0.205	0.132	0.082	-0.146	-0.024	0.216
ETH	0.096	0.005	0.077	-0.083	-0.021	0.066
Summit	0.154	0.064	0.055	-0.042	-0.016	0.020
Humboldt	0.081	0.061	0.028	-0.099	-0.054	0.060
TUNU	0.187	0.150	0.039	0.103	0.032	0.048

At TUNU-N, the multiangular approach performs rather well (differences less than approximately 3%). However, at this station, the multispectral approach results in surface albedo that are, on average, 15% less than the station measurements. The *in situ* measurements at this site show albedo values that range from 0.92–0.97. Very new snow could result in a surface albedo of 0.92 over the spectral range corresponding to the LI–COR measurements, but values near 0.97 are suspect. The primary source of error in the *in situ* measurements is instrument level [20]. Although all the station data have been quality controlled [20] and the instruments are releveled every 1–2 years to minimize errors due to instrument level, problems with instrument level likely remain in the data. Table III summarizes the maximum, mean, and standard deviations of the differences between the satellite-derived and station-measured albedo at each station.

VI. DISCUSSION

Required broadband albedo accuracies for climate modeling purposes are 0.05 [19]. Since the broadband albedo for moderately bright snow is around 0.80, this would require the albedo to be known to within about 6%. The results in Table III show that, in general, the satellite-derived albedo is within 6% of the station measurements, although there are a few cases where the albedo error exceeds this value. Overall, the statistical model based on the angular information of the red MISR channel performs better than the method based on the MISR spectral information. This is to be expected because the LI–COR data were directly used in developing the statistical model, and, therefore, the albedo using this method should more accurately represent the LI–COR measurements than the other method, which aims to derive an albedo over a "broader" spectral range. An advantage of the statistical model is that it is developed directly using the MISR HDRF data, and thus errors in the instrument calibration and atmospheric correction are imbedded directly into the statistical model.

In contrast, the albedo-retrieval method based on the spectral information is subject to several possible sources of error, including calibration errors, errors in the atmospheric correction,

errors in the BRDF conversion factors, and errors in the narrowband-to-broadband albedo conversion. These error sources are discussed in more detail below. Other sources of discrepancy between the satellite-derived and *in situ* measurements are a result of errors in the *in situ* albedo, cloud-contamination, surface roughness effects, and spatial inhomogeneity.

A. Accuracy of Sensor Calibration

Calibration of the MISR instrument is performed using calibration coefficients computed from a time trend analysis, considering the preflight, on-board calibrator (OBC), and overflight measurements. MISR radiances are optimized over all radiances for which OBC calibration data are acquired (1–70% in reflectance). Since launch, several different calibration algorithms have been used. During the time period for which the July and August 2000 data were collected, the calibration coefficients for the An red and NIR bands caused the reflectances to be about 3% brighter than actually believed to be the case. In addition, the fore–aft camera radiances were biased by a few percent.

For the June 2001 data, a new quadratic calibration equation was used to convert the sensor data to radiance values. This algorithm may change the radiances reported over dark targets, by a few percent, but does not compromise the fit at higher radiance levels. On July 11, 2001, separate calibration coefficients were developed for the photodiodes, as they view the north panel (used for aft and AN-red and NIR channels) and the south panel (used for the fore and AN-blue, green channels). This change is expected to improve fore–aft camera biases. However, it is currently unclear if the absolute calibration is within 5%. The data used in this study are either in the "beta" or "provisional" phases, which means that performance of the instrument and the science processing are still being investigated by the MISR team. Therefore, the accuracy of the calibration of the data used in this study may not be optimal.

A 10% calibration error in any one channel would translate into approximately a 10% error in the surface HDRF and the surface spectral albedo. However, in terms of the broadband albedo, the impact will depend on which channel is affected and if more than one channel is affected. To test this, we modeled the narrowband and broadband albedo for a variety of snow and atmospheric conditions. Model inputs included different snow grain sizes varying from 250–1000 μm, as well as a variety of atmospheric conditions (arctic summer and winter models, aerosol optical depth from 0.01–0.10, and four different aerosol models). The modeled narrowband albedo for each channel was then increased by 10%.

Errors in the narrowband surface albedo can propagate into large errors in the broadband albedo. For the MISR narrowband-to-broadband albedo model of [15], the largest broadband albedo error is found when the NIR narrowband albedo is in error. In this case, a 10% error in the NIR albedo translates into a broadband albedo error of 4%. For a 10% error in the other channels, the error in the broadband albedo is less than 3%. However, it is also entirely possible that more than one channel may be in error, resulting in different broadband albedo errors. For example, if all the MISR channels are in error by 10%, the error in the MISR broadband albedo is also approximately 10%.

B. Accuracy of Atmospheric Correction

The accuracy of the atmospheric correction depends in part on the accuracy with which the atmospheric constituents can be determined and the sensitivity of the correction to uncertainty in these variables. The main atmospheric variables used as input into 6S are the profiles of atmospheric water vapor and ozone and the aerosol optical depth. The type of aerosol model selected also plays a part. In general, the visible and NIR channels used in this study are not very sensitive to changes in atmospheric water vapor and ozone. The Chappuis ozone absorption band between 0.45 and 0.75 μm will affect spectral bands that lie within this wavelength region. However, increasing the ozone amount by 50% only results in a change in TOA BRF within the Chappuis absorption band of 1–3%, depending on the specific sun-sensor viewing geometry. Larger differences are found for oblique viewing and solar zenith angles.

Similarly, the atmospheric water vapor has little impact on the TOA BRF used in this study. The water vapor absorption band at 0.94 μm will affect MISR band 4 (NIR). However, the effect on this band is usually less than 1% for a 50% change in column atmospheric water vapor amount.

Greater sensitivity is observed for aerosol optical depth and, to a lesser extent, the aerosol type and properties. Since snow is brighter than the path radiance, aerosols have a net darkening effect over snow. Depending on the type of aerosol model used, the decrease is mostly linear (such as for the continental aerosol model used in this study) for low solar and satellite zenith angles. For more oblique angles, the decrease of reflectance with increasing aerosol optical depth becomes less linear. The visible spectral channels are more sensitive to changes in aerosol optical depth than the NIR channels. Decreases of 6% in the blue and green TOA BRF can be found for changes in aerosol optical depth from 0.01–0.1 using the continental aerosol model. Larger differences are observed for a more strongly absorbing aerosol model, such as an urban aerosol model.

C. Accuracy of Conversion Factors

One means to test how well the conversion factors perform is to examine if any angular dependence remains in the albedo after applying the conversion factors. Theoretically, if the conversion factors accurately portray the angular signature of the snow surface, there would be no dependence of the albedo on the viewing or azimuth angles.

The MISR data provide a good opportunity to test how well the conversion factors perform, since the surface is viewed at nine discrete angles. Fig. 5(a) and (b) shows the TOA BRF, the surface HDRF, and the surface albedo for August 12, 2000, at the ETH/CU camp (a) and August 25, 2000, at Summit (b). If the conversion factors were "correct," the red spectral albedo would be constant over the different viewing angles in both the fore and aft directions. However, we find that the fore and aft cameras sometimes have significantly different surface albedo. On August 12, 2000, at the ETH/CU camp, the difference in red albedo between the Da and Df cameras is only 0.05 and gives an example where the conversion factors worked relatively well. On August 25, 2000, at Summit, however, the difference between the Da and Df red cameras is 0.17. Thus, problems

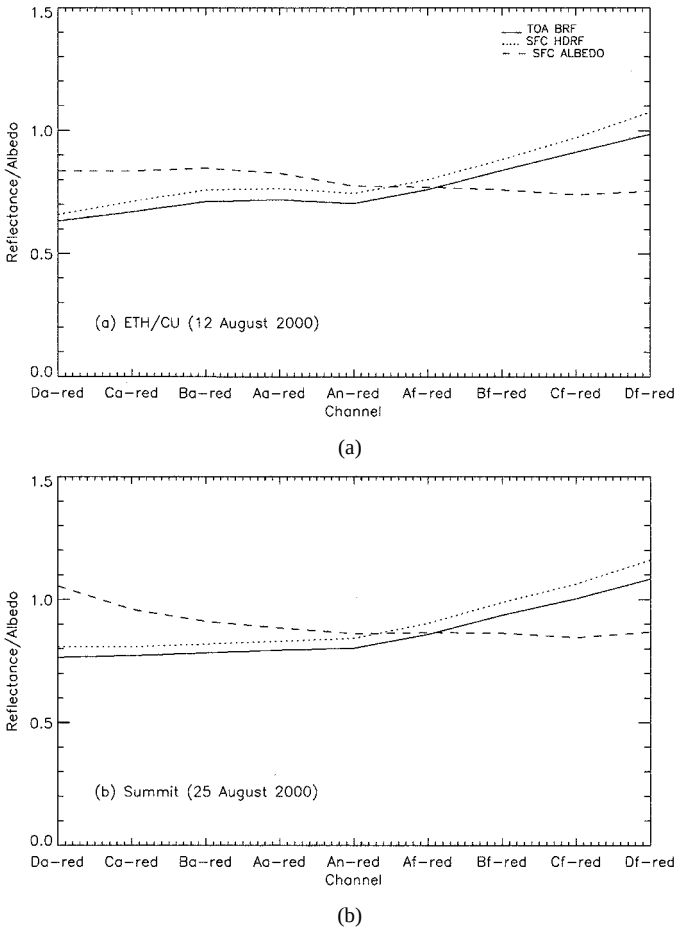

Fig. 5. TOA bidirectional reflectance factor (BRF) (solid line), surface HDRF (dotted line), and surface spectral albedo (dashed line) for MISR on August 12, 2000, at the ETH/CU camp (a) and August 25, 2000, at Summit (b).

likely still remain in the snow BRDF model used to derive the conversion factors, especially at oblique viewing angles. Since only nadir reflectances were used in deriving the surface albedo from the MISR spectral data, we believe that errors from the conversion factors are reduced.

Also, the presence of melt ponds, wet firn, and a rough surface can lead to errors in the conversion factors used here. Mie theory assumes that the particles are spherical, and DISORT assumes that the surface is flat and uniform. Another possibility for error in the conversion factors is that the diffuse component of the atmosphere is not well modeled. More diffuse sky radiation than what we modeled with 6S would reduce the overcorrection found at the extreme fore and aft angles. It is also important to remember that camera-to-camera biases likely remain because of MISR calibration errors. Thus, it is difficult to adequately access the accuracy of the snow BRDF model and, hence, the conversion factors. More data are needed to further study how well the model performs.

D. Accuracy of Narrowband-to-Broadband Conversion

One of the reasons why published narrowband-to-broadband relationships differ widely is that they are dependent upon both surface and atmospheric conditions. Thus, to develop a more general model, a variety of surface and atmospheric conditions are needed. Modeling results over Greenland suggest that any linear narrowband-to-broadband relationship is dependent on the snow grain size, solar zenith angle, and the atmospheric profiles of water vapor and ozone. For small aerosol optical depths (e.g., less than 0.12), a linear model is valid as long as the solar zenith angles are not greater than about 70°. For turbid atmospheres, modeling results suggest that a nonlinear model is more appropriate.

Another problem that exists with developing the multiple linear regression models is that the independent variables (e.g., the narrowband albedos) are highly correlated with each other, with the unfortunate result that the narrowband-to-broadband albedo model may perform badly when implemented on future data. This was discovered when using some Greenland *in situ* data to develop a multiple linear regression model and then applying it to the MISR data. Very poor results were achieved at JAR and ETH/CU during the summer melt period. Multicollinearity may also result in negative values of the regression coefficients, leading to negative predicted broadband albedo. One means to deal with the multicollinearity of the independent variables is to use principle components as predictors in place of the narrowband albedos. This will be investigated in the near future.

VII. Conclusions

This paper compared satellite-retrieved surface albedo with ground-based measurements of snow albedo at five different sites in Greenland. Two different techniques were developed and used to derive the surface albedo: one based on the spectral information from the MISR instrument and one using the angular information from MISR.

In general, the surface albedo derived from the two different methods using the MISR instrument showed good agreement with the *in situ* data (within about 6%). In addition, both methods yielded similar results, following the downward trends in the surface albedo at the JAR and ETH/CU sites as a result of increased ablation during the summer season and little variability at the other sites. Agreement was slightly better using the angular statistical model to derive the albedo, but this is expected, since the LI–COR measured albedo were used directly in developing the statistical model.

At this point, it is not possible to say which method gives better overall results. Further validation with more MISR imagery is needed to make any conclusive statements about the performance of either method. The angular information of the MISR data does, however, appear capable of capturing the general variability and magnitude of the surface albedo. The advantage of developing such a statistical model is the relative ease with which such a model can be implemented.

Acknowledgment

MISR data were provided through the NASA Langley Distributed Active Archive Center (DAAC). Special thanks to B. Gaitley at JPL for processing of the sunphotometer data, to J. Box at University of Colorado for processing of the AWS station data, and to the anonymous reviewers for their careful and constructive reviews.

REFERENCES

[1] J. Stroeve, A. Nolin, and K. Steffen, "Comparison of AVHRR-derived and *in situ* surface albedo over the Greenland ice sheet," *Remote Sens. Environ.*, vol. 62, pp. 262–276, 1997.

[2] W. H. Knap and J. Oerlemans, "The surface albedo of the Greenland ice sheet: Satellite-derived and in situ measurements in the Søndre Strømfjord area during the 1991 melt season," *J. Glaciol.*, vol. 42, no. 141, pp. 364–374, 1996.

[3] De Abreu, J. Key, J. A. Maslanik, M. C. Serreze, and E. F. LeDrew, "Comparison of in situ and AVHRR-derived broadband albedo over Arctic sea ice," *Arctic*, vol. 47, no. 3, pp. 288–297, 1994.

[4] A. G. Klein and D. K. Hall, "Snow albedo determination using the NASA MODIS instrument," in *Proc. East. Snow Conf.*, Fredericton, NB, Canada, June 2–4, 1999, pp. 77–85.

[5] A. Nolin, F. Fetterer, and T. C. Scambos, "Surface roughness characterizations of sea ice and ice sheets: Case studies with MISR data," *IEEE Trans. Geosci. Remote Sensing*, vol. 40, pp. 1605–1615, July 2002.

[6] J. V. Martonchik, D. J. Diner, B. Pinty, M. M. Verstraete, R. B. Myneni, Y. Knayazikhin, and H. R. Gordon, "Determination of land and ocean reflective, radiative, and biophysical properties using multiangle imaging," *IEEE Trans. Geosci. Remote Sensing*, vol. 36, pp. 1266–1281, July 1998.

[7] K. Steffen, J. E. Box, and W. Abdalati, "Greenland Climate Network: GC-Net." In "Special Report on Glaciers, Ice Sheets and Volcanoes, tribute to M. Meier," CRREL, Rep. 96-27, S. C. Colbeck, Ed., 1996.

[8] J. C. Stroeve, J. E. Box, C. Fowler, T. Haran, and J. Key, "Intercomparison between in situ and AVHRR polar pathfinder-derived surface albedo over Greenland," *Remote Sens. Environ.*, vol. 75, pp. 360–374, 2001.

[9] S. Liang, "Narrowband to broadband albedo conversions of land surface albedo I—Algorithms," *Remote Sens. Environ.*, vol. 76, pp. 213–239, 2001.

[10] D. Tanre, B. N. Holben, and Y. J. Kaufman, "Atmospheric correction algorithm for NOAA–AVHRR products: Theory and application," *IEEE Trans. Geosci. Remote Sensing*, vol. 30, pp. 231–248, Mar. 1992.

[11] S. G. Warren, R. E. Brandt, and P. O. 'Rawe Hinton, "Effects of surface roughness on bidirectional reflectance of Antarctic snow," *J. Geophys. Res.*, vol. 103, pp. 25789–25807, 1998.

[12] K. Stamnes, S.-C. Tsay, W. Wiscombe, and K. Jayaweera, "Numerically stable algorithm for discrete-ordinate-method radiative transfer in multiple scattering and emitting layered media," *Appl. Opt.*, vol. 27, pp. 2502–2509, 1988.

[13] Z. Li and H. G. Leighton, "Narrowband to broadband conversion with spatially autocorrelated reflectance measurements," *J. Appl. Meteorol.*, vol. 31, pp. 421–431, 1992.

[14] R. W. Lindsay and D. A. Rothrock, "Arctic sea ice albedo from AVHRR," *J. Climate*, vol. 7, pp. 1737–1749, 1994.

[15] W. H. Knap, C. H. Reijmer, and J. Oerlemans, "Narrowband to broadband conversion of Landsat TM glacier albedos," *Int. J. Remote Sens.*, vol. 20, pp. 2091–2110, 1999.

[16] J.-L. Roujean, M. Leroy, and P.-Y. Deschamps, "A bidirectional reflectance model of the Earth's surface for the correction of remote sensing data," *J. Geophys. Res.*, vol. 97, pp. 20455–20468, 1992.

[17] W. Lucht, C. B. Schaaf, and A. H. Strahler, "An algorithm for the retrieval of albedo from space using semiempirical BRDF models," *IEEE Trans. Geosci. Remote Sensing*, vol. 38, pp. 977–998, Mar. 2000.

[18] B. Pinty and M. M. Verstraete, "On the design and validation of surface bidirectional reflectance and albedo models," *Remote Sens. Environ.*, vol. 41, pp. 155–167, 1992.

[19] A. Henderson-Sellers and M. F. Wilson, "Surface albedo data for climate modeling," *Rev. Geophys. Space Phys.*, vol. 21, pp. 1743–1778, 1983.

[20] J. Box, "personal communication," .

Julienne C. Stroeve received the Ph.D. degree from the Department of Geography and the Cooperative Institute for Research in Environmental Studies (CIRES), University of Colorado, Boulder, in 1996, with a thesis on the radiation climatology of the Greenland ice sheet using visible and thermal satellite imagery.

She joined The National Snow and Ice Data Center (NSIDC), Boulder, CO, after graduation. She is currently a Data Coordinator and Team Leader for passive microwave sea ice and polar atmospheric data sets archived and distributed by NSIDC. Her current research projects involve validation and development of snow albedo algorithms from the Advanced Very High Resolution Radiometer (AVHRR), the Moderate Resolution Imaging Spectroradiometer (MODIS), and the Multi-angle Imaging SpectroRadiometer (MISR) instruments. Other projects involve analysis of seasonal and interannual variations of surface albedo and temperature for Greenland, validation of snow surface temperature from the Advanced Along Track Scanning Radiometer (AATSR), surface albedo and grain size determination from EO-1 instruments, and sensitivity studies of sea ice passive microwave brightness temperatures to variations in surface and atmospheric conditions to help improve current sea ice models and data assimilation.

Anne W. Nolin received the B.A. degree in anthropology and the M.S. degree in soils, water, and engineering from the University of Arizona, Tucson, in 1980 and 1987, respectively. She received the Ph.D. degree in geography from the University of California, Santa Barbara, in 1993.

She is currently a Member of the MISR Science Team at the Jet Propulsion Laboratory, Pasadena, CA. She has worked as a Research Scientist at the Cooperative Institute for Research in Environmental Sciences and the National Snow and Ice Data Center at the University of Colorado, Boulder, since 1993. Her research interests include integrating studies of snow, hydrology, and climate with innovative methods of satellite observation.

Dr. Nolin is a member of the Association of American Geographers, the American Meteorological Society, the International Glaciological Society, and the American Geophysical Union. As part of the MISR Science Team, she received a NASA Group Achievement Award.